

A fast bioluminescent source localization method based on generalized graph cuts with mouse model validations

Kai Liu¹, Jie Tian^{a,1,2}, Yujie Lu³, Chenghu Qin¹, Xin Yang¹,
Shouping Zhu¹, Xing Zhang¹

¹Medical Image Processing Group, Institute of Automation, Chinese Academy of Sciences,
P. O. Box 2728, Beijing, 100190, China

²Life Science Center, Xidian University, Xian, Shaanxi 710071, China

³Crump Institute for Molecular Imaging, Department of Molecular and Medical
Pharmacology, David Geffen School of Medicine at UCLA, Los Angeles, CA 90095, USA

tian@ieee.org

Abstract: Bioluminescence imaging (BLI) makes it possible to elucidate molecular and cellular signatures to better understand the effects of human disease in small animal models *in vivo*. The unambiguous three-dimensional bioluminescent source information obtained by bioluminescence tomography (BLT) could further facilitate its applications in biomedicine. However, to the best of our knowledge, the existing gradient-type reconstruction methods in BLT are inefficient, and often require a relatively small volume of interest (VOI) for feasible results. In this paper, a fast generalized graph cuts based reconstruction method for BLT is presented, which is to localize the bioluminescent source in heterogeneous mouse tissues via max-flow/min-cut algorithm. Since the original graph cuts theory can only handle graph-representable problem, the quadratic pseudo-boolean optimization is incorporated to make the graph representable and tractable, which is called generalized graph cuts (GGC). The internal light source can be reconstructed from the whole domain, so *a priori* knowledge of VOI can be avoided in this method. In the simulation validations, the proposed method was validated in a heterogeneous mouse atlas, and the source can be localized reliably and efficiently by GGC; and compared with gradient-type method, the proposed method is about 25-50 times faster. Moreover, the experiments for sensitivity to the measurement errors of tissue optical properties demonstrate that, the reconstruction quality is not much affected by mismatch of parameters. In what follows, *in vivo* mouse BLT reconstructions further demonstrated the potential and effectiveness of the generalized graph cut based reconstruction method.

© 2010 Optical Society of America

OCIS codes: (170.6960) Tomography; (100.3190) Inverse problem; (170.3660) Light propagation in tissues; (170.6280) Spectroscopy, fluorescence and luminescence

References and links

1. R. Weissleder and M. J. Pittet, "Imaging in the era of molecular oncology," *Nat.* **452**, 580–589 (2008).
2. J. K. Willmann, N. van Bruggen, L. M. Dinkelborg, and S. S. Gambhir, "Molecular imaging in drug development," *Nat. Rev. Drug Discov.* **7**, 591–607 (2008).

3. V. Ntziachristos, J. Ripoll, L. V. Wang, and R. Weissleder, "Looking and listening to light: the evolution of whole body photonic imaging," *Nat. Biotechnol.* **23**, 313–320 (2005).
4. B. W. Rice, M. D. Cable, and M. B. Nelson, "In vivo imaging of lightemitting probes," *J. Biomed. Opt.* **6**, 432–440 (2001).
5. M. Jiang and G. Wang, "Image reconstruction for bioluminescence tomography," *Proc. SPIE*, **5535**, 335–351 (2004).
6. X. Gu, Q. Zhang, L. Larcom, and H-B. Jiang, "Three dimensional bioluminescence tomography with model based reconstruction," *Opt. Express* **12**, 3996–4000 (2004), <http://www.opticsinfobase.org/oe/abstract.cfm?URI=OPEX-12-17-3996>.
7. W-X. Cong, G. Wang, D. Kumar, Y. Liu, M. Jiang, L. V. Wang, E. Hoffman, G. McLennan, P. McCray, J. Zabner, and A. Cong, "Practical reconstruction method for bioluminescence tomography," *Opt. Express* **13**, 6756–6771 (2005), <http://www.opticsinfobase.org/oe/abstract.cfm?id=140930>.
8. G. Wang, H-O. Shen, W-X. Cong, S. Zhao, and G-W. Wei, "Temperature-modulated bioluminescence tomography," *Opt. Express* **14**, 7852–7871 (2006), <http://www.opticsinfobase.org/oe/abstract.cfm?uri=oe-13-18-6756>.
9. G. Alexandrakis, F. R. Rannou, and A. F. Chatzioannou, "Tomographic bioluminescence imaging by use of a combined optical-PET (OPET) system: a computer simulation feasibility study," *Phys. Med. Biol.* **50**, 4225–4241 (2005).
10. W-X. Cong, D. Kumar, L. V. Wang, and G. Wang, "A Born-type approximation method for bioluminescence tomography," *Med. Phys.* **33**, 679–686 (2006).
11. G. Wang, W-X. Cong, K. Durairaj, X. Qian, H-O. Shen, P. Sinn, E. Hoffman, G. McLennan, and M. Henry, "In vivo mouse studies with bioluminescence tomography," *Opt. Express* **14**, 7801–7809 (2006), <http://www.opticsinfobase.org/abstract.cfm?URI=oe-14-17-7801>.
12. N. V. Slavine, M. A. Lewis, E. Richer, and P. P. Antich, "Iterative reconstruction method for light emitting sources based on the diffusion equation," *Med. Phys.* **33**, 61–68 (2006).
13. Y-J. Lv, J. Tian, G. Wang, W-X. Cong, J. Luo, W. Yang, and H. Li, "A multilevel adaptive finite element algorithm for bioluminescence tomography," *Opt. Express* **14**, 8211–8223 (2006), <http://www.opticsinfobase.org/abstract.cfm?URI=oe-14-18-8211>.
14. A. J. Chaudhari, F. Darvas, J. R. Bading, R. A. Moats, P. S. Conti, D. J. Smith, S. R. Cherry, and R. M. Leahy, "Hyperspectral and multispectral bioluminescence optical tomography for small animal imaging" *Phys. Med. Biol.* **50**, 5421–5441 (2005).
15. H. Dehghani, S. C. Davis, S. Jiang, B. W. Pogue, K. D. Paulsen, and M.S. Patterson, "Spectrally resolved bioluminescence optical tomography," *Opt. Lett.* **31**, 365–367 (2006).
16. Y-J. Lv, J. Tian, H. Li, W-X. Cong, G. Wang, W-X. Yang, C-H. Qin, and M. Xu, "Spectrally resolved bioluminescence tomography with adaptive finite element: methodology and simulation," *Phys. Med. Biol.* **52**, 4497–4512 (2007).
17. C. Kuo, O. Coquoz, T. L. Troy, H. Xu, and B. W. Rice, "Three-dimensional reconstruction of in vivo bioluminescent sources based on multispectral imaging," *J. Biomed. Opt.* **12**, 024007:1–12 (2007).
18. S. Ahn, A. J. Chaudhari, F. Darvas, C. A. Bouman, and R. M. Leahy, "Fast iterative image reconstruction methods for fully 3D multispectral bioluminescence tomography," *Phys. Med. Biol.* **53**, 3921–3942 (2008).
19. J-C. Feng, K-B. Jia, C-H. Qin, G-R. Yan, S-P. Zhu, X. Zhang, J-T. Liu, and J. Tian, "Three-dimensional Bioluminescence Tomography based on Bayesian Approach," *Opt. Express* **17**, 16834–16848 (2009), <http://www.opticsinfobase.org/oe/abstract.cfm?uri=oe-17-19-16834>.
20. Y-J. Lu, H. B. Machado, A. Douraghy, D. Stout, H. Herschman and A. F. Chatzioannou, "Experimental bioluminescence tomography with fully parallel radiative-transfer-based reconstruction framework," *Opt. Express* **17**, 16681–16695 (2009), <http://www.opticsinfobase.org/abstract.cfm?URI=oe-17-19-16681>.
21. V. Kolmogorov and R. Zabih, "What energy functions can be minimized via graph cuts?" *IEEE Trans. Patt. Anal. and Mach. Intell.* **26**, 147–159 (2004).
22. Y. Boykov and V. Kolmogorov, "An experimental comparison of min-cut/max-flow algorithms for energy minimization in vision," *IEEE Trans. Patt. Anal. and Mach. Intell.* **26**, 1124–1137 (2004).
23. V. Kolmogorov and C. Rother, "Minimizing nonsubmodular functions with graph cuts-a review," *IEEE Trans. Patt. Anal. and Mach. Intell.* **9**, 1274–1279 (2007).
24. Y. Boykov, O. Veksler, and R. Zabih, "Efficient approximate energy minimization via graph cuts," *IEEE Trans. Patt. Anal. and Mach. Intell.* **20**, 1222–1239 (2001).
25. V. Lempitsky, C. Rother, S. Roth, and A. Blake, "Fusion moves for markov random field optimization," *IEEE Trans. Patt. Anal. and Mach. Intell.*, in press.
26. G. Wang, Y. Li, and M. Jiang, "Uniqueness theorems in bioluminescence tomography," *Med. Phys.* **31**, 2289–2299 (2004).
27. P. L. Hammer, P. Hansen, and B. Simeone, "Roof duality, complementation and persistency in quadratic 0-1 optimization," *Math. Program.* **28**, 121–155 (1984).
28. L. Ford and D. Fulkerson, "Maximal flow through a network," *Canad. J. Math.* **8**, 309–404 (1956).
29. A. V. Goldberg and R. E. Tarjan, "A new approach to the maximum-flow problem," *J. ACM* **35**, 921–940 (1988).
30. G-R. Yan, J. Tian, S-P. Zhu, Y-K. Dai, and C-H. Qin, "Fast cone-beam CT image reconstruction using GPU

- hardware,” *J. X-Ray Sci. and Technol.* **16**, 225–234 (2008).
31. S-P. Zhu, J. Tian, G-R. Yan, C-H. Qin, and J-C. Feng, “Cone beam micro-CT system for small animal imaging and performance evaluation,” *Int. J. Biomed. Imaging*, doc. ID 960573 (2009).
 32. X. Zhang, J. Tian, J-C. Feng, S-P. Zhu, and G-R. Yan, “An anatomical mouse model for multimodal molecular imaging,” presented at 31st International Conference of the IEEE Engineering in Medicine and Biology Society, Hilton Minneapolis, Minnesota, USA, September 2–6, 2009.
 33. V. Ntziachristos, A. H. Hielscher, A. G. Yodh, and B. Chance, “Diffuse optical tomography of highly heterogeneous media,” *IEEE Trans. Med. Imaging* **20**, 470–478 (2001).
 34. G. Alexandrakis, F. R. Rannou, and A. F. Chatziioannou, “Effect of optical property estimation accuracy on tomographic bioluminescence imaging: simulation of a combined optical-PET (OPET) system,” *Phys. Med. Biol.* **51**, 2045–2053 (2006).
 35. J. Virostko, A. C. Powers, and E. D. Jansen, “Validation of luminescent source reconstruction using single-view spectrally resolved bioluminescence images,” *App. Opt.* **46**, 2540–2547 (2007).
-

1. Introduction

Bioluminescence imaging (BLI) has become a promising modality in cancer research, cell trafficking and drug development [1, 2, 3]. There is no inherent tissue autofluorescence generated by external excitation light, making it extremely sensitive [4]. Furthermore, bioluminescence tomography (BLT) can make use of the information obtained from BLI data measured on the surface of a small animal in reference to a corresponding micro-CT volume of the same small animal, and localize the bioluminescent source deep in tissue.

Over the past few years, many reconstruction methods for BLT have been developed. To the best of our knowledge, they are mainly gradient-type methods [5, 6, 7, 8, 9, 10, 11, 12, 13, 14, 15, 16, 17, 18, 19]. Since it has to execute many iteration steps and calculate the gradient in every iteration until reliable results are obtained, the time cost during the reconstruction is relatively expensive [18]. Parallel computation is one way to improve the reconstruction efficiency, but it needs expensive and complex hardware to support the corresponding algorithm [20]. Furthermore, many of the existing methods are apt to adopt relatively small volume of interest (VOI, it can also be called permissible region), which is known prior to the BLT reconstruction. Nevertheless, it is not always reliable or feasible to define such a region effectively [8]. Especially, for the cases on a large VOI or even on the whole region, the results may be trapped in local extremum and be very far from the optimal solutions.

Here, a gradient-free reconstruction method is presented, which is called generalized graph cuts (GGC). Graph-cuts-based technique is emerging as an increasingly useful method for energy minimization in computer vision including segmentation, image restoration and stereo [21, 22, 23, 24, 25]. In the field of BLT problem, firstly, a tractable graph with nonnegative edge weights is constructed. Then, a max-flow/min-cut approach is applied to localize the bioluminescent source. Because the max-flow/min-cut is not dependent on gradient any more, it can perform very efficiently. Moreover, by restricting graph representable, the global optimal solutions can be often found in polynomial time [22]. Therefore, the graph cuts method can provide both fast and exact solutions.

The outline of the paper is as follows. In the next section, we present the reconstruction methodology for BLT. In the beginning, the diffusion approximation for the radiative transfer equation is briefly introduced. And then, the generalized graph cuts based reconstruction method is elaborately formulated. In order to make the graph generated by the BLT problem representable, the quadratic pseudo-boolean optimization is applied to transform the graph tractable, which can be found in the second subsection. In Section 3, the simulation verifications are demonstrated for the proposed method. Firstly, numerical reconstruction comparisons between GGC and a gradient-type method demonstrate the efficiency and reliability of the proposed method in a heterogeneous mouse atlas. In what follows, the sensitivity to the measurement errors of tissue optical properties with different source locations are also con-

sidered. Experimental BLT reconstructions further show the potential and effectiveness of the GGC based reconstruction method for practical bioluminescence imaging. Finally, we conclude the paper in the last section.

2. Methodology

2.1. Diffusion model

In the steady-state domain, the forward problem of light propagation for BLT can be modeled as a diffusion equation [7, 11], which is given by

$$-\nabla \cdot (D(\mathbf{r})\nabla(\Phi(\mathbf{r}))) + \mu_a(\mathbf{r})\Phi(\mathbf{r}) = \mathcal{X}(\mathbf{r}) \quad (\mathbf{r} \in \Omega) \quad (1)$$

with a Robin-type boundary condition:

$$\Phi(\mathbf{r}) + 2\kappa(\mathbf{r}, n, n')D(\mathbf{r})(\mathbf{v}(\mathbf{r}) \cdot \nabla\Phi(\mathbf{r})) = 0 \quad (\mathbf{r} \in \partial\Omega) \quad (2)$$

Here Ω and $\partial\Omega$ denote region of the object and the boundary of the region respectively, Φ the flux density, \mathcal{X} an isotropic source term, μ_a the absorption coefficient μ_s the scattering coefficient, $D = 1/[3(\mu_a + (1-g)\mu_s)]$ the optical diffusion coefficient, g the anisotropy parameter, and \mathbf{v} the unit outward normal on $\partial\Omega$. $\kappa(\mathbf{r}, n, n')$ is a function that represents refractive index mismatched between tissue and the surrounding medium, and $\kappa(\mathbf{r}, n, n') = [1 + R(\mathbf{r}, n, n')]/[1 - R(\mathbf{r}, n, n')]$, where n the refractive index with Ω and n' in the surrounding medium. In the experiment, the medium surrounding Ω is air, for which $n' \approx 1$. Therefore, $R(\mathbf{r}, n, n')$ can be approximated by $R \approx 1.4399n^{-2} + 0.7099n^{-1} + 0.6681 + 0.0636n$ [7]. The measured quantity is the outgoing photon density on $\partial\Omega$ [7]:

$$V(\mathbf{r}) = -D(\mathbf{r})(\mathbf{v}(\mathbf{r}) \cdot \nabla\Phi(\mathbf{r})) = \frac{\Phi(\mathbf{r})}{2\kappa(\mathbf{r}, n, n')} \quad (3)$$

After generating the matrix-vector equation by finite element formulation of Eqs. (1) and (2), the linear relationship between the measured photon density distribution and the unknown source distribution deep in mouse tissue is established [7]:

$$\mathcal{M}\mathcal{X} = \Phi \quad (4)$$

where \mathcal{M} denotes the system matrix in finite element formulation, and Φ the photon density on the boundary.

2.2. Generalized graph cuts based reconstruction method

Due to the highly ill-posed nature, BLT is an extremely intractable inverse problem [26]. The common approach uses the output-least-squares formulation incorporated with a regularization term. The solution can be determined by minimizing the energy function:

$$\min E(\mathcal{X}) = \min \|\mathcal{M}\mathcal{X} - \mathbf{b}\|^2 + \lambda \|\mathcal{X}\|^2 \quad (5)$$

where \mathbf{b} is the measured photon density on the boundary, and λ the regularization parameter. In this paper, the generalized graph cuts reconstruction method is presented. In the content of standard graph cuts theory, first of all, a directed graph $\mathcal{G} = (\mathcal{V}, \mathcal{A})$ needs to be created. Set $\mathcal{V} = \{i | i \in \text{FE-grid}\} \cup \{s, t\}$, where i denotes the nodes in the finite-element grid (FE-grid) of the whole region of object, and s and t are special suppositional source and sink respectively, which are called the terminals. Set \mathcal{A} represents both the edges on the FE-grid and the edges

between the terminals and the nodes on the grid (as shown in Fig. 1(a)) [24]. Then, energy function (5) is reformulated into the graph framework as follows:

$$\begin{aligned} E(\mathcal{X}) &= \|\mathcal{M}\mathcal{X} - \mathbf{b}\|^2 + \lambda\|\mathcal{X}\|^2 \\ &= \theta_{const} + \sum_{i \in \mathcal{V}} \theta_i(x_i) + \sum_{(i,j) \in \mathcal{A}} \theta_{ij}(x_i, x_j) \end{aligned} \quad (6)$$

where

$$\mathcal{M} = [\mathbf{m}_1, \mathbf{m}_2, \dots, \mathbf{m}_N] \quad (7)$$

and

$$\begin{cases} \theta_{const} &= \mathbf{b}^T \mathbf{b} & (8a) \\ \theta_i(x_i) &= (\mathbf{m}_i^T \mathbf{m}_i + \lambda)x_i^2 - 2(\mathbf{b}^T \mathbf{m}_i)x_i & (8b) \\ \theta_{ij}(x_i, x_j) &= 2(\mathbf{m}_i^T \mathbf{m}_j)x_i x_j & (8c) \end{cases}$$

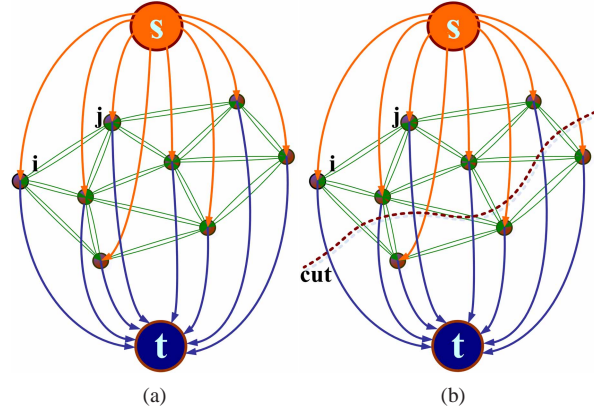


Fig. 1: An irregular directed graph and the cut. (a) A graph \mathcal{G} . (b) A cut on graph \mathcal{G} . It is noted that the mesh is constructed by tetrahedron elements, so graph used here is not regular any more and the adjacent connections of each node become very complex.

here \mathbf{m}_i is the i -th column vector of \mathcal{M} , $\mathcal{X} = \{x_i\}$ (x_i is value of the node i), N denotes the number of nodes, θ_{const} is the constant term of the energy, $\theta_i(\cdot)$ are the unary terms which denotes the weight of the edges between the nodes on the grid and the terminals, and $\theta_{ij}(\cdot, \cdot)$ are the pairwise terms, which denotes the weight of the edges between the nodes on the grid. Unfortunately, the conventional graph cuts can only be used for minimizing *submodular* energy functions, i.e. functions whose pairwise terms satisfy [21]

$$\theta_{ij}(0,0) + \theta_{ij}(1,1) \leq \theta_{ij}(0,1) + \theta_{ij}(1,0) \quad (9)$$

and minimizing *supermodular* energy functions, whose pairwise terms stand by

$$\theta_{ij}(0,0) + \theta_{ij}(1,1) > \theta_{ij}(0,1) + \theta_{ij}(1,0) \quad (10)$$

In order to minimize energy functions with both *submodular* in Eq. (9) and *supermodular* terms in Eq. (10) via graph theory, the quadratic pseudo-boolean optimization is employed

[27]. It has four useful properties: a) *Persistency* which implies that the energy never goes up. b) *Partial optimality* which guarantees there exists global minimum \mathcal{E}^* of energy in Eq. (6) such that $x_i = x_i^*$ for all labeled nodes i . c) This algorithm is invariant with respect to “flipping” a subset of nodes $\mathcal{U} \subset \mathcal{V}$, which means that flipping transforms *supermodular* terms between \mathcal{U} and $\mathcal{V} \setminus \mathcal{U}$ into *submodular*. d) If all terms of the energy are *submodular*, then the algorithm will label all nodes.

Motivated by the properties aforementioned, the original graph can be revised as follows. For each node $i \in \mathcal{V}$ there will be two nodes i and \bar{i} . Node \bar{i} can be associated with variable $x_{\bar{i}}$. Therefore, $V = \{i, \bar{i} | i \in \mathcal{V}\} \cup \{s, t\}$. Moreover, for every non-zero term of $\theta_{ij}(\cdot, \cdot)$, two edges are added to the set A [23]. Then the graph represents energy E' expressed as a function of old variables \mathcal{X} and new variables $\bar{\mathcal{X}} = \{x_{\bar{i}}\}$ [27]:

$$\begin{aligned}
 E'(\mathcal{X}, \bar{\mathcal{X}}) = \theta_{const} &+ \frac{1}{2} \sum_{i \in \mathcal{V}} [\theta_i(x_i) + \theta_i(1 - x_{\bar{i}})] \\
 &+ \frac{1}{2} \sum_{(i,j) \in Sub} [\theta_{ij}(x_i, x_j) + \theta_{ij}(1 - x_{\bar{i}}, 1 - x_{\bar{j}})] \\
 &+ \frac{1}{2} \sum_{(i,j) \in Super} [\theta_{ij}(x_i, 1 - x_{\bar{j}}) + \theta_{ij}(1 - x_{\bar{i}}, x_j)] \quad (11)
 \end{aligned}$$

Now, a new directed graph $G_q = (V, A)$ has been constructed and the size of this graph is doubled, and the generalized graph cuts method is established. Here, *Sub* and *Super* denote the sets in which the terms are *submodular* and *supermodular*, respectively. According to the properties above, the minimum of the energy would be obtained via GGC. In addition, since the new energy E' of variables $\{x_i, x_{\bar{i}}\}$ is enforced to be *submodular*, it can be minimized in polynomial time [22]. According to the theorem of Ford and Fulkerson [28], the computation

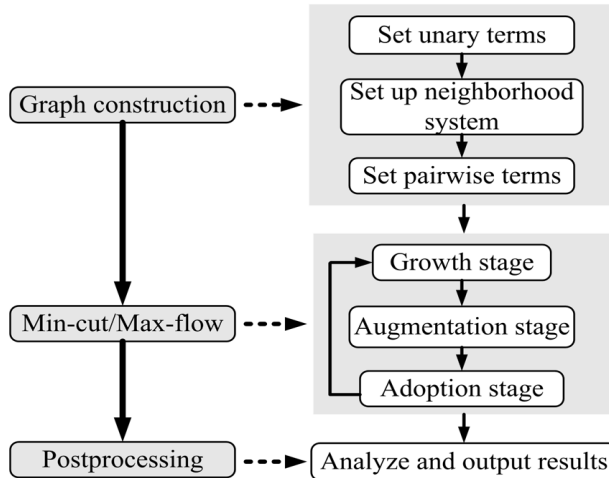


Fig. 2: The GGC algorithmic structure used for BLT reconstruction.

of the min-cut is equivalent to computing the max-flow from the source to the sink. Several algorithms can compute this flow [22, 24, 29]. One of the powerful graph cuts is Boykov-Kolmogorov’s algorithm, which belongs to augmenting path-based type. Normally, it starts a new search for $s \rightarrow t$ paths as soon as all paths of a given length are exhausted [22]. It is noted

that, for certain optimization problems like BLT, max-flow/min-cut algorithms can provide a fast and exact solution. The algorithm presented here involves three parts: graph construction, min-cut/max-flow, and postprocessing, as shown in Fig. 2. Firstly, graph should be constructed by setting unary and pairwise terms, and setting up the neighborhood system. It needs to be emphasized that unlike the graphs used in the context of computer vision and image segmentation, etc. [22, 24], the graphs in bio-optics are usually irregular in three dimension (Fig. 1(a)), so adjacent connections of the nodes via edges should be built up. Secondly, min-cut/max-flow is executed by iteratively repeating three stages: growth, augmentation, and adoption [22]. After the adoption stage is completed, it returns to the growth stage. The algorithm terminates when the search trees on the graph cannot grow and the graph is separated by saturated edges. This implies that a maximum flow is achieved, and the corresponding min-cut is generated, as shown in Fig. 1(b). Finally, the results are analyzed and output.

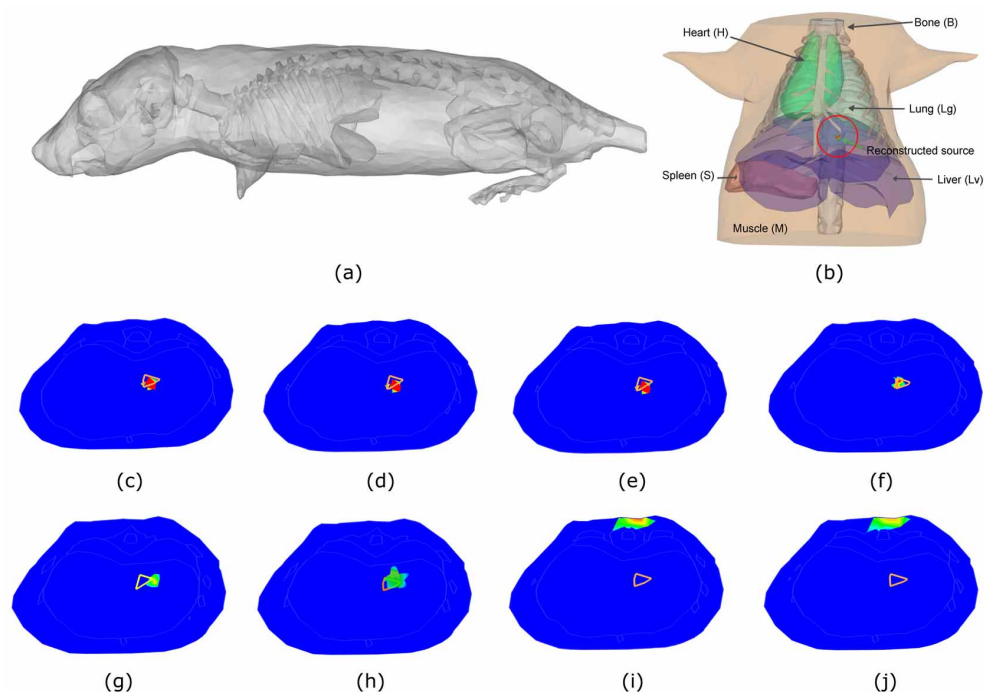


Fig. 3: The comparison of tomographic results between GGC and gradient-type method when the bioluminescent source is located at about the mouse torso center and no measurement error of tissue optical properties exists. (a) Mouse phantom captured by CT imaging system. (b) Mouse torso used for reconstructions and the 3D tomographic results based on GGC on the whole region of torso (4614 nodes). The arrow points to the reconstructed source in liver. (c)-(f) The results in 2D of the proposed method for 536, 1097, 3453 and 4614 nodes in the corresponding VOIs (Table 2), respectively. (g)-(j) are the counterparts with the gradient-type method. All the reconstructed values above zero in the slices are displayed in the results. The filled patch is the reconstructed source, and the other is the real one.

3. Results

3.1. Numerical verifications

3.1.1. Reconstruction comparison between generalized graph cuts and gradient-type methods

Before reconstructions, the anatomical structure of the BALB/c mouse was developed using our micro-CT system and cone-beam reconstruction algorithm (Fig. 3(a)) [30, 31]. By using image processing and interactive segmentation methods [32], several primary organs were delineated, and the optical coefficients for each organ were estimated using the method in Ref. [9], as listed in Table 1. Since the segmented organs are mainly in the torso, this part was used for image reconstructions. This mouse atlas was discretized into volumetric mesh, which contains 25783 tetrahedral elements and 4614 nodes with 486 nodes on the surface. The actual source was located at about torso center, with the coordinate of (21.45, 33.65, 14.52) in liver and the physical dimension of 1.48mm.

Table 1: Optical properties for each organ in the mouse atlas. The units are mm^{-1} .

	Heart	Lung	Liver	Spleen	Muscle	Bone
μ_a	0.022	0.071	0.128	0.075	0.032	0.0024
μ_s	1.129	2.305	0.646	2.178	0.586	0.935

In the numerical reconstructions, four cases with different size of VOI were considered (Table 2), and a constrained Newton-type optimization method was selected as a gradient-based method [13], and employed to compare with GGC based method. In all cases of GGC of this part, as shown in Figs. 3(b)-(f), the location error from the real source is within 0.5mm, and the size of VOI has little effect to the reconstructed results. The dimension of the recovered source also fairly matches with that of real one. Even on the whole atlas, which means none *a priori* knowledge about source distribution is incorporated (Figs. 3(b) and (f)), the position and dimension of the source can still be accurately recovered by GGC. In contrast, the reconstructed locations using the gradient-based method offset more from the real one, and when the VOI enlarges, the offset becomes greater in Fig. 3(g) compared with (h), or even the recovered position is too far from the real one to be acceptable (Figs. 3(i) and (j)).

Moreover, compared with gradient-based, GGC is 25-50 times faster, and according to the reconstruction time (the total time for the three parts in Fig. 2) in Table 3 and Fig. 4, the efficiency of GGC becomes increasingly remarkable as more and more nodes and edges appear. Therefore, it is convincing that the GGC method is obviously advantageous over its counterpart both in efficiency and accuracy. The regularization parameters in this part were selected in the domain of $5 \times 10^{-4} - 5 \times 10^{-3}$. All reconstructions in this paper were implemented using C++ and performed on a desktop computer with Intel Core 2 Duo 1.86GHz CPU and 3GB RAM.

Table 2: The volume of interest used the in comparisons.

VOI	Nodes	Edges	Region
1	536	1183	$\{(x, y, z) \mid 17 \geq z \geq 12 \text{ and } 35 \geq y \geq 29 \text{ and lung}\}$
2	1097	3989	$\{(x, y, z) \mid 18 \geq z \geq 10 \text{ and } 35 \geq y \geq 25 \text{ and lung}\}$
3	3453	21372	$\{(x, y, z) \mid 23 \geq z \geq 8\}$
4	4614	30880	$\{(x, y, z) \mid \text{the point in the whole region}\}$

Table 3: Comparisons of reconstruction results between GGC and a gradient-type method. Loc. Error denotes the distance between the center of real source and the center of reconstructed one.

VOI	Method	Recons. Loc. Center (mm)	Loc. Error (mm)	Dimension (mm)	Recons. Time (s)
1	GGC	(21.53, 33.56, 14.97)	0.47	1.26	1.55
	Grad.-type	(23.34, 34.98, 14.30)	2.44	2.36	46.35
2	GGC	(21.53, 33.56, 14.97)	0.47	1.29	7.24
	Grad.-type	(23.34, 34.98, 14.23)	2.33	2.46	264.42
3	GGC	(21.53, 33.56, 14.97)	0.47	1.29	80.35
	Grad.-type	(27.03, 33.31, 14.07)	5.61	4.18	2087.32
4	GGC	(21.33, 33.54, 14.88)	0.39	1.22	148.78
	Grad.-type	(27.56, 33.66, 15.47)	6.74	3.88	5639.25

3.1.2. Sensitivity to the measurement errors of tissue optical properties

As one kind of *a priori* information, optical properties of mouse tissues are essential for reducing the ill-posedness and maintaining uniqueness of BLT [9, 26]. During the simultaneous optical property measurement process, however, there is inevitable discrepancies between the detected optical properties of the *in vivo* small animals and the actual physiological values, which may affect the tomographic localization of bioluminescent source. Currently, the quantification accuracy of diffusive optical tomography (DOT) can achieve a range of about 10-50% error depending on various factors [33]. In this part, $\pm 50\%$ errors for all tissues were considered in BLT reconstructions.

Two cases were involved to examine the sensitivity to the measurement errors of tissue optical properties of the proposed method. In the first case, the bioluminescent source was placed at about half-radius position in the mouse torso, with the center of (18.75, 34.01, 16.05) in liver and the physical dimension of 1.33mm. The second one was the same as above-mentioned in Section 3.1.1. All the reconstructions were performed on the whole atlas region.

When the source was located at half-radius position, the desirable reconstructed results for both the underestimation and overestimation of optical properties were similar with that in Figs. 5 based on normal ones, which means no measurement error of tissue optical properties exists (as shown in Figs. 6(a) and (c)). The location error for the cases of normal and $\pm 50\%$ errors were restricted within 1mm, as listed in Table 4. It is reported that, as the source depth increased, the optical property errors increasingly affects the BLT reconstruction quality [34]. However, using the proposed method, reliable results at the center of the mouse torso was reconstructed when $\pm 50\%$ optical property errors were considered for all tissues, as shown in Figs. 6(c) and (d). In this case, the localization errors for normal and $\pm 50\%$ optical errors were also restricted within 1mm (Table 4), and unlike the effects in Ref. [34], the ring-like shape results did not appear in the reconstruction. Moreover, it is very interesting that both in two cases of the torso center and half-radius, the dimension error of +50% error for all tissues is larger than -50% error, also as listed in Table 4. For all the reconstruction process in this part, the time cost is about 150s. It is shown that the proposed method is non-sensitive to the measurement errors of optical properties, and it is capable for tolerating errors to get desirable results using almost the same time cost.

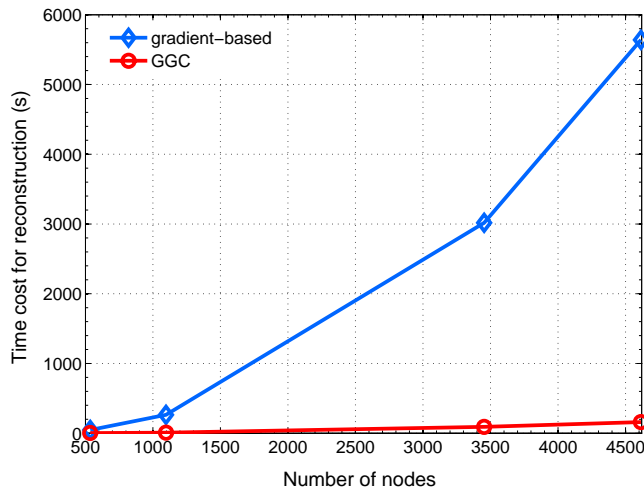


Fig. 4: Time cost comparisons between GGC and a gradient-type method for BLT reconstructions. The grid used here contains 486 nodes on the surface of the mouse atlas. The execution time of the proposed method grows much more slowly with the number of nodes than that of the latter.

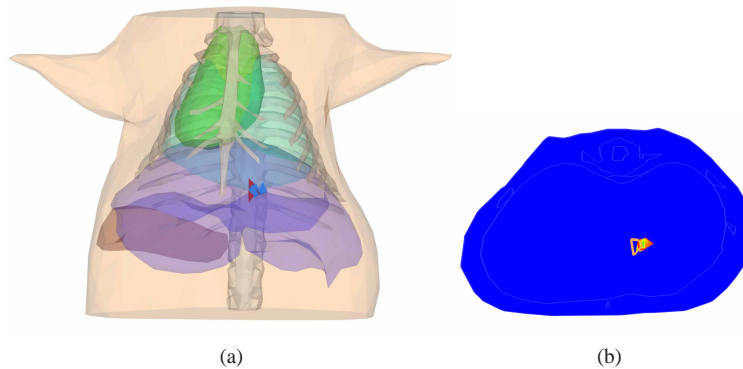


Fig. 5: The tomography results based on GGC on the whole region when the bioluminescent source is located at about the half-radius of the mouse torso and no measurement error of tissue optical properties exists. (a) The results in 3D. All the reconstructed values above zero in the slices are displayed in the results. (b) The corresponding results in 2D.

Table 4: Reconstruction results with different source locations and measurement errors of tissue optical properties. All the results were reconstructed on the whole region.

	Opt. Prop. Error	Recons. Loc. Center (mm)	Loc. Error (mm)	Dimension (mm)	Recons. Time (s)
1	normal	(19.47, 34.13, 16.12)	0.72	1.37	149.53
	+50%	(19.17, 33.89, 15.90)	0.46	2.01	147.17
	-50%	(19.61, 34.29, 16.12)	0.91	1.56	146.32
2	normal	(21.33, 33.54, 14.88)	0.39	1.22	150.79
	+50%	(21.68, 34.55, 14.57)	0.92	2.51	148.65
	-50%	(21.52, 34.19, 15.27)	0.92	1.73	147.02

3.2. Experimental reconstructions based on generalized graph cuts

To further verify the generalized graph cuts based reconstruction method, mouse experiments were performed on a Maestro 2 *in vivo* imaging system (CRI, Woburn, Massachusetts). This system uses a cooled CCD camera and a liquid crystal tunable filter to acquire the optical data. To simulate a known bioluminescent source, a luminescent bead (Mb-Microtec, Bern, Switzerland) was used with an emission spectrum similar to that of a firefly luciferase-based source. In this bead, tritium is used to excite a phosphor that generates photons, making it a very stable calibrated source. Its dimension is 0.9mm in diameter and 2.5mm long. A mutant hairless mouse (SKH1-hr, Charles River, San Diego, CA) was used in this experiment, as shown in Fig. 7(a).

Before performing the experiment, the mouse was anesthetized and the bead was surgically inserted into the mouse body. Since the light can only penetrate from the dorsal view, the optical data was acquired in single-view. The exposure time for each wavelength was 5min to obtain high signal-to-noise. After finishing the optical signal acquisition, the mouse was scanned using the Imtek micro-CT system to obtain the surface and volumetric shape of the mouse. The CT data was used to generate volumetric mesh for image reconstruction. And then, the optical data was registered with the volumetric mesh for measured data mapping. Figure 7(b) shows the volumetric mesh used in this reconstruction and the mapped photon distribution on the mouse surface. This mesh contains 21550 tetrahedral elements and 4322 discretized nodes with 1252 nodes on the surface. Since the photon propagation path is almost totally consisted of muscle tissue, we assumed that the reconstructed domain was homogeneous with muscle tissue. The corresponding optical properties was used in reconstruction: $\mu_a=0.187mm^{-1}$ and $\mu_s'=0.929mm^{-1}$ [35]. The tritium source was easily distinguished in CT images and we could confirm that the actual center of the source was (45.00, 52.60, -10.15).

Figure 8 shows the reconstructed results of the GGC based method. As is shown, the reconstructed center position of the source is (45.30, 52.20, -8.80). Although the reconstructed source was very close to the actual source position, there was a little difference between the experimental reconstructions and the simulations (as in Section 3.1), especially in the direction of z. The main reason leading this offset is the imaging artifacts caused by respiration of the mouse. Another factor maybe the bladder-like regions in the mouse body, which can cause non-scattering effect. Additionally, the complexity of *in vivo* mouse tissues also arouses some discrepancies of reconstructed image when the whole reconstruction region is regarded as homogenous media. The reconstruction time for the mesh is 358.21s. Nevertheless, it is still illustrated that the proposed reconstruction method is potential for experimental reconstructions. This further demonstrates its high efficiency and capability to localize the source on whole region reliably.

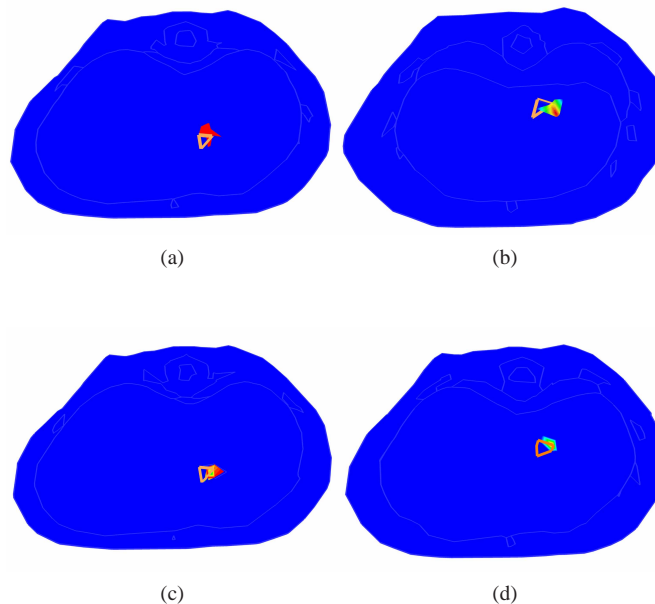


Fig. 6: The tomographic results with the proposed method in view of sensitivity to optical property errors based on GGC. (a) and (c) The reconstructed results corresponding to +50% and -50% optical property errors for all tissues respectively when the bioluminescent sources were located at about half-radius position in the mouse torso. (b) and (d) The reconstructed results corresponding to +50% and -50% optical property errors for all tissues respectively when the bioluminescent sources were located at about center of the mouse torso. All the reconstructed values above zero in the slices are displayed in the results.

4. Conclusion

In this paper, a generalized graph cuts approach for localizing the bioluminescent source in mouse is presented. Since the standard graph cuts theory can only handle graph-representable problem, the quadratic pseudo-boolean optimization is incorporated to transform the *supermodular* terms into *submodular* ones. Thus, the revised graph becomes tractable and can be used in BLT problem.

In the numerical verifications, firstly, reconstruction comparisons between GGC and gradient-based method demonstrate accuracy and efficiency of the proposed method. Based on the proposed method, even no *a priori* knowledge of small VOI is used, the desirable results can still be reconstructed precisely (e.g. Figs. 3(b), (f) and Figs. 5(a)-(b)). Secondly, a set of reconstructions were considered to test the sensitivity to the measurement errors of tissue optical properties. Although the disagree of +50% optical error for all tissues is larger than that of -50% error with respect to the recovered dimension of sources, both the sources at the center and half-radius of mouse torso with 50% underestimation and overestimation of optical properties can be reliably reconstructed. Moreover, the experimental reconstructions further show the possibility of the GGC method for complex *in vivo* mouse BLT applications.

In conclusion, we have developed a generalized graph cuts based approach for localizing the bioluminescent source on whole region. Simulations and experimental verifications demonstrated that BLT reconstructions based on the proposed method can acquire good source lo-

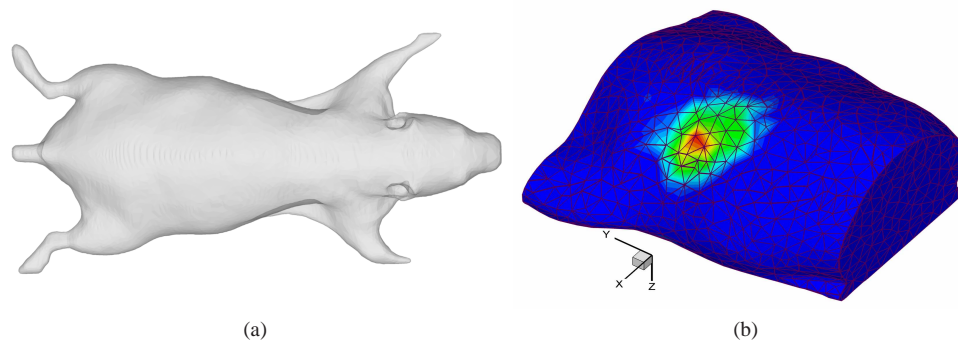


Fig. 7: The mouse profile and the mesh. (a) The mouse profile in bioluminescence imaging. (b) The volumetric mesh of the mouse torso used for imaging reconstructions and the mapped photon distribution on the mouse surface.

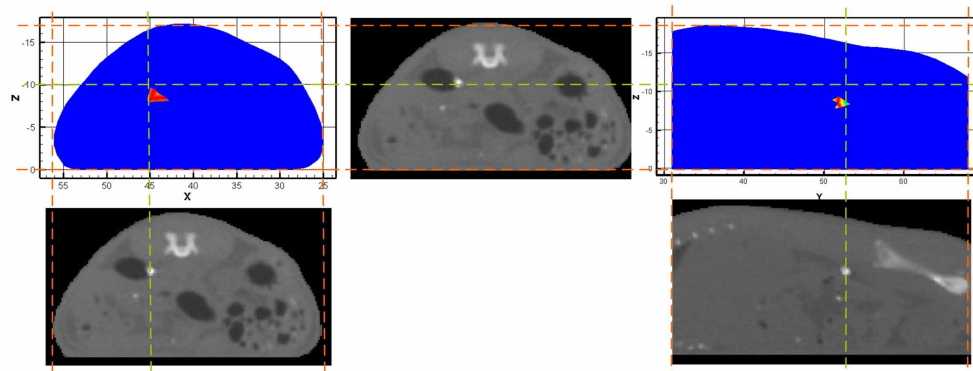


Fig. 8: The experimental BLT reconstructions with the proposed method. The results are shown in lateral and vertical cross sectional views, compared with the source location in the corresponding CT slices. It is noted that all the reconstructed values above zero in the slices are displayed for the results.

calization, as well as much higher efficiency and lesser dependency on *a priori* information, making it potential for practical mouse study in BLT and other optical imaging modalities. In future, further research will focus on GGC method based on other more precise forward models and real mouse experiments with tumor models and the relevant bioluminescence probes.

Acknowledgments

The authors would like to thank Arion F Chatzioannou from David Geffen School of Medicine at UCLA for the mouse data, Prof. Vladimir Kolmogorov from Computer Science Department of University College London, Prof. Olga Veksler from Computer Science Department of University of Western Ontario, and Carsten Rother from Computer Vision Group at Microsoft Research Cambridge for beneficial discussions. They also gratefully acknowledge the support by the National Basic Research Program of China (973) under Grant No. 2006CB705700, Program Changjiang Scholars and Innovative Research Team in University (PCSIRT) under Grant No. IRT0645, CAS Hundred Talents Program, CAS scientific research equipment develop pro-

gram under Grant No. YZ200766, the Knowledge Innovation Project of the Chinese Academy of Sciences under Grant Nos. KGCX2-YW-129, KSCX2-YW-R-262, the National Natural Science Foundation of China under Grant Nos. 30672690, 30600151, 60532050, 60621001, 30873462, 60910006, 30970769, 30970771, Beijing Natural Science Fund under Grant No. 4071003, Technology Key Project of Beijing Municipal Education Commission under Grant No. KZ200910005005.